PROCEEDINGS OF SCIENCE

CP Violation in $B \to K\ell^+\ell^-$ Decays: New Opportunities in the High-Precision Era

Robert Fleischer,[a,b] **Eleftheria Malami,**[a,c] **Anders Rehult**[a,b,*] **and K. Keri Vos**[a,d]

[a] *Nikhef, Science Park 105, NL-1098 XG Amsterdam, Netherlands*
[b] *Department of Physics and Astronomy, Vrije Universiteit Amsterdam, NL-1081 HV Amsterdam, Netherlands*
[c] *Center for Particle Physics Siegen (CPPS), Theoretische Physik 1, Universität Siegen, D-57068 Siegen, Germany*
[d] *Gravitational Waves and Fundamental Physics (GWFP), Maastricht University, Duboisdomein 30, NL-6229 GT Maastricht, the Netherlands*

E-mail: arehult@nikhef.nl

Experimental data on rare B-meson decays indicate deviations from Standard Model predictions. In studies of these decays, new sources of CP violation are often neglected. We discuss CP violation in the rare B-meson decays $B \to K\ell^+\ell^- (\ell = \mu, e)$ and point to two phenomena that arise when new sources of CP violation are included. First, the Wilson coefficients $C_{9\ell}$ and $C_{10\ell}$ become complex, and we show how we can extract their values from measurements of direct and mixing-induced CP asymmetries. Second, new sources of CP violation can generate nontrivial lepton flavour universality violation. Such violation is usually measured through ratios like R_K and R_{K^*}, but we show that measuring only these ratios leaves a large parameter space unexplored. These results bring exciting opportunities to reveal New Physics effects in the high-precision era.

Corfu Summer Institute 2023 "School and Workshops on Elementary Particle Physics and Gravity" (CORFU2023)
23 April - 6 May , and 27 August - 1 October, 2023
Corfu, Greece

*Speaker

PoS(CORFU2023)128

1. Introduction

The decays $B \to K\ell^+\ell^- (\ell = \mu, e)$ belong to the class of rare B-meson decays, which in the Standard Model (SM) occur only at the loop level and are heavily suppressed. For this reason they are excellent probes of New Physics (NP). Rare B-meson decays have recently received a lot of attention in the literature (see e.g. [1–10]), much of it owing to LHCb's observation that the branching ratio of $B \to K\mu^+\mu^-$ is lower than the SM prediction, with a statistical significance of $\sim (3-4)\sigma$ [11, 12].

If this deviation is confirmed to be caused by NP, the next step is to identify what that NP is. In the language of Effective Field Theory (EFT), NP is encoded in the Wilson coefficients that enter the decay. If we can extract the values of these coefficients, we can match an EFT to different high-energy theories to see which theories can explain the observed deviation. These coefficients are often assumed to be real numbers, but in general they can be complex. If they are, they encode new sources of CP violation beyond the SM. We will show how measurements of CP asymmetries in $B^\pm \to K^\pm\mu^+\mu^-$ and $B_d^0 \to K_S\mu^+\mu^-$ decays can be used to extract the complex values of the relevant Wilson coefficients.

Another indication of NP was until recently given by the ratio

$$R_K = \frac{\Gamma(B^- \to K^-\mu^+\mu^-) + \Gamma(B^+ \to K^+\mu^+\mu^-)}{\Gamma(B^- \to K^-e^+e^-) + \Gamma(B^+ \to K^+e^+e^-)}, \tag{1}$$

which probes universality between muons and electrons. For several years, measurements of this ratio deviated from the SM value of unity [13–16]. However, as of December 2022, the value is in agreement with the SM prediction [17–19]. Does this mean that electron–muon universality is now tightly constrained in $B \to K\ell^+\ell^-$? As we will show, that is not the case: With new CP-violating phases entering the decays, we can still have electron–muon non-universality even with $R_K \sim 1$. We will discuss CP-violating observables that offer exciting new perspectives at the high-precision frontier.

2. Theoretical framework

2.1 Effective Hamiltonian

For $b \to s\ell^+\ell^-$ transitions, the relevant low-energy effective Hamiltonian is [20–23]

$$\mathcal{H}_{\text{eff}} = -\frac{4G_F}{\sqrt{2}}\left[\lambda_u\left\{C_1(O_1^c - O_1^u) + C_2(O_2^c - O_2^u)\right\} + \lambda_t\sum_{i\in I} C_i O_i\right], \tag{2}$$

where $\lambda_q = V_{qb}V_{qs}^*$ are CKM factors and $I = \{1c, 2c, 3, 4, 5, 6, 8, 7^{(\prime)}, 9^{(\prime)}\ell, 10^{(\prime)}\ell, S^{(\prime)}\ell, P^{(\prime)}\ell, T^{(\prime)}\ell\}$. We neglect the doubly Cabibbo-suppressed terms, which contribute at the $O(\lambda^2) \sim 5\%$ level, and consider the following operators:

$$\begin{aligned}
O_{7^{(\prime)}} &= \frac{e}{(4\pi)^2} m_b[\bar{s}\sigma^{\mu\nu}P_{R(L)}b]F_{\mu\nu}, & O_{S^{(\prime)}\ell} &= \frac{e^2}{(4\pi)^2} m_b[\bar{s}P_{R(L)}b](\bar{\ell}\ell),\\
O_{9^{(\prime)}\ell} &= \frac{e^2}{(4\pi)^2}[\bar{s}\gamma^\mu P_{L(R)}b](\bar{\ell}\gamma_\mu\ell), & O_{P^{(\prime)}\ell} &= \frac{e^2}{(4\pi)^2} m_b[\bar{s}P_{R(L)}b](\bar{\ell}\gamma_5\ell),\\
O_{10^{(\prime)}\ell} &= \frac{e^2}{(4\pi)^2}[\bar{s}\gamma^\mu P_{L(R)}b](\bar{\ell}\gamma_\mu\gamma_5\ell), & O_{T^{(\prime)}\ell} &= \frac{e^2}{(4\pi)^2}[\bar{s}\sigma^{\mu\nu}P_{R(L)}b](\bar{\ell}\sigma_{\mu\nu}\ell),
\end{aligned} \tag{3}$$

with $P_{R(L)} = \frac{1}{2}(1 \pm \gamma_5)$ and $\sigma_{\mu\nu} = \frac{i}{2}[\gamma_\mu, \gamma_\nu]$. The index ℓ indicates lepton flavour. We will suppress that label it when it is clear from context that a specific flavour is considered. Furthermore, all Wilson coefficients C_i should in the rest of this write-up be understood as a shorthand for $C_i + C_i'$.

2.2 Observables

We will work with three observables: Branching ratios, direct CP asymmetries, and mixing-induced CP asymmetries. For detailed expressions, see [12]. We define the q^2-integrated direct CP asymmetry of $B^\pm \to K^\pm\mu^+\mu^-$ as

$$\mathcal{A}_{\rm CP}^{\rm dir}[q^2_{\rm min}, q^2_{\rm max}] = \frac{\bar{\Gamma}[q^2_{\rm min}, q^2_{\rm max}] - \Gamma[q^2_{\rm min}, q^2_{\rm max}]}{\bar{\Gamma}[q^2_{\rm min}, q^2_{\rm max}] + \Gamma[q^2_{\rm min}, q^2_{\rm max}]} , \tag{4}$$

where $\bar{\Gamma} \equiv \Gamma(B^- \to K^-\ell^+\ell^-)$ and $\Gamma \equiv \Gamma(B^+ \to K^+\ell^+\ell^-)$, with

$$\Gamma[q^2_{\rm min}, q^2_{\rm max}] = \int_{q^2_{\rm min}}^{q^2_{\rm max}} \frac{d\Gamma}{dq^2} dq^2 . \tag{5}$$

In contrast to charged B-meson decays, which have only direct CP violation, neutral B-meson decays can also show mixing-induced CP violation. This phenomenon arises through $B^0_q - \bar{B}^0_q$ oscillations if the B^0_q and $\bar{B}^0_q$ mesons can both decay into the same final state. Here, we consider the decay $B^0_d \to K_S\ell^+\ell^-$. We define the mixing-induced CP asymmetry through the time-dependent decay rate [24]:

$$\frac{\Gamma(B^0_q(t) \to f) - \Gamma(\bar{B}^0_q(t) \to f)}{\Gamma(B^0_q(t) \to f) + \Gamma(\bar{B}^0_q(t) \to f)} = \frac{-\mathcal{A}_{\rm CP}^{\rm dir}\cos(\Delta M_q t) - \mathcal{A}_{\rm CP}^{\rm mix}\sin(\Delta M_q t)}{\cosh\left(\frac{\Delta\Gamma_q}{2}t\right) + \mathcal{A}_{\Delta\Gamma}\sinh\left(\frac{\Delta\Gamma_q}{2}t\right)} , \tag{6}$$

where $\mathcal{A}_{\rm CP}^{\rm mix}$ is the mixing-induced CP asymmetry and $\mathcal{A}_{\rm CP}^{\rm dir}$ is the direct CP asymmetry of (4). Here, $\Delta\Gamma_q = \Gamma^q_H - \Gamma^q_L$ is decay width difference between the heavy and light B_q mass eigenstates, and $\Delta M_q = M^q_H - M^q_L$ is the mass difference.

The direct and mixing-induced CP asymmetries can be generated through complex phases in C_9 and/or C_{10}. The two asymmetries have complementary sensitivities to these coefficients: The direct asymmetry depends only C_9, while the mixing-induced one depends on both C_9 and C_{10}. We will now use this fact to extract the CP-violating phases of the two coefficients.

3. Extracting complex Wilson coefficients from CP asymmetries

In this section, based on [12], we show how CP asymmetries in $B \to K\mu^+\mu^-$ allow us to extract the complex values of C_9 and C_{10}. We first discuss the relevant experimental bounds, then demonstrate how the CP-violating observables give us complementary information, and finally extract the values of C_9 and C_{10} in a fit to hypothetical data from a future benchmark scenario.

3.1 Experimental bounds

For the branching ratio we use data from [11], while we use [25] for the direct CP asymmetry. We will begin by focusing on the q^2 bin of $[7, 8]$ GeV^2, where the LHCb collaboration finds

$$\mathcal{B}(B^+ \to K^+\mu^+\mu^-)[7, 8] = (23.1 \pm 1.8) \times 10^{-9} \tag{7}$$

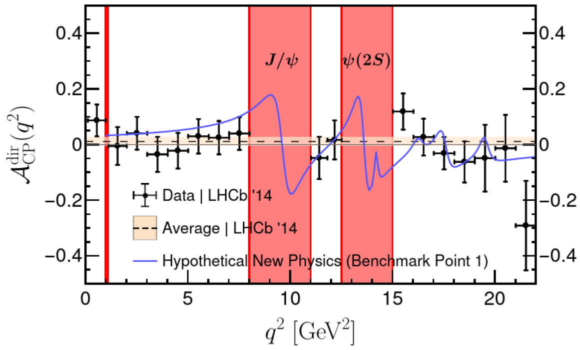

Figure 1: Experimental data on the direct CP asymmetry of $B^- \to K^-\mu^+\mu^-$ from the LHCb collaboration [25]. The blue line indicates a theory prediction following Benchmark Point 1 of (10). (From [12]. Similar figures can be found in [26, 27].)

and [25]

$$\mathcal{A}^{\rm dir}_{\rm CP}[7,8] = 0.041 \pm 0.059\ . \tag{8}$$

In Fig. 1, we show data on the direct CP asymmetry in different q^2-bins. We focus on the small bin of [7, 8] GeV^2 because it is near the J/ψ resonance at $m^2_{J/\psi} = 9.6\,\text{GeV}^2$, where the direct CP asymmetry could be enhanced [26]. Concerning the mixing-induced asymmetry, there are not yet any data. For SM predictions of all these observables, see [12].

For illustration, we consider three NP scenarios, which all fit the current rare B-meson decay data better than the SM [4, 7–10]:

$$\begin{aligned} &\text{Scenario 1:} \quad C_9^{\rm NP} \neq 0\,, \\ &\text{Scenario 2:} \quad C_9^{\rm NP} = -C_{10}^{\rm NP} \neq 0\,, \\ &\text{Scenario 3:} \quad C_{10}^{\rm NP} \neq 0\,. \end{aligned} \tag{9}$$

Fig. 2 shows the 1σ experimental bounds on the complex Wilson coefficients of our three scenarios. The oval regions are bounds from the branching ratio, while the light orange ones come from the direct CP asymmetry. The colour gradients follow the magnitudes of NP contributions. For these plots we have used a CKM input following [28] that combines a value of $|V_{ub}|$ from exclusive semileptonic B decays with a value of $|V_{cb}|$ from inclusive ones. We have also assumed a model of hadronic long-distance effects from [29] (see [12] for a detailed discussion). We have indicated by a star and diamond two benchmark points that are allowed by the data but still have large CP-violating phases:

$$\begin{aligned} &\text{Benchmark Point 1:} \quad |C_9^{\rm NP}|/|C_9^{\rm SM}| = 0.75\,, \qquad \phi_9^{\rm NP} = 195^\circ\,, \\ &\text{Benchmark Point 2:} \quad |C_9^{\rm NP}|/|C_9^{\rm SM}| = |C_{10}^{\rm NP}|/|C_9^{\rm SM}| = 0.30 \quad \phi_9^{\rm NP} = \phi_{10}^{\rm NP} - \pi = 220^\circ\,. \end{aligned} \tag{10}$$

The blue line in Fig. 1 shows how Benchmark Point 1 leads to an enhanced CP asymmetry near $c\bar{c}$ resonances, following [26]. This enhancement also occurs for Benchmark Point 2, but to a smaller degree. We will use these points in Section 3.3.

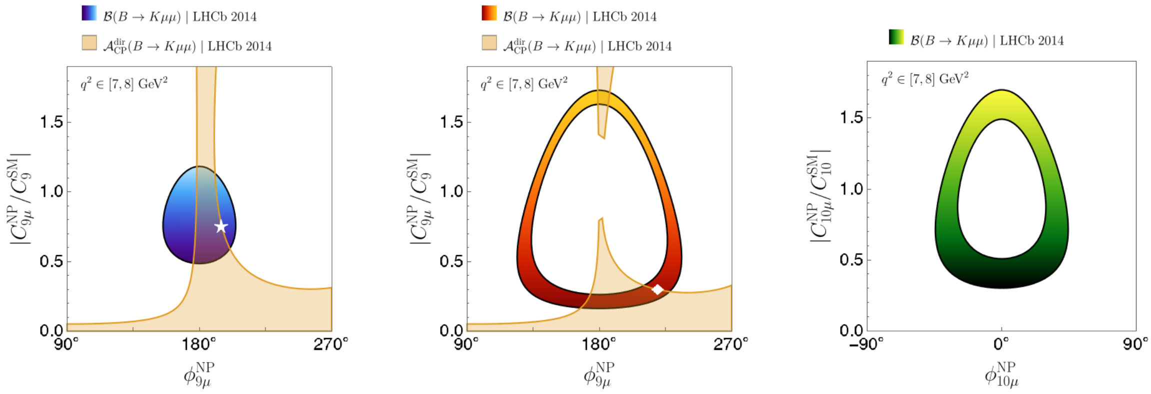

(a) $C_9^{\rm NP}$ only **(b)** $C_9^{\rm NP} = -C_{10}^{\rm NP}$ **(c)** $C_{10}^{\rm NP}$ only

Figure 2: Experimental 1σ bounds on the three NP scenarios of (9). The star and diamond indicate Benchmark Points 1 and 2 of (10), respectively. The colour gradients follow the magnitudes of the Wilson coefficients. (From [12].)

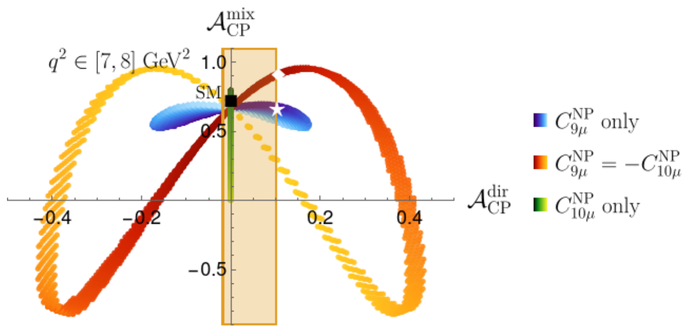

Figure 3: Correlations between direct and mixing-induced CP asymmetries in $B_d \to K_S\mu^+\mu^-$ in the three NP scenarios of (9). The orange vertical band marks the current experimental bound on the direct CP asymmetry. The colours for each scenario correspond to Fig. 2 and indicate magnitudes of Wilson coefficients: Lighter colours indicate larger magnitudes. (From [12].)

3.2 Correlations between CP-violating observables

Through correlations between the direct and mixing-induced CP asymmetries of $B_d \to K_S\mu^+\mu^-$, we can distinguish between the three NP scenarios of (9). Folding the experimentally allowed regions of Fig. 2 onto the $(\mathcal{A}_{\rm CP}^{\rm dir}, \mathcal{A}_{\rm CP}^{\rm mix})$ plane, we obtain the correlations of Fig. 3. In this plane, each NP scenario leaves a distinct "fingerprint", with different allowed values. In Scenario 1, the direct CP asymmetry can take any value within $[-0.2, 0.2]$ while the mixing-induced CP asymmetry stays close to the SM prediction. In Scenario 2, we get much larger asymmetries, with direct CP asymmetries as large as ± 0.4 and mixing-induced ones in $[-0.8, 0.9]$. In Scenario 3, the direct CP asymmetry is always zero, while the mixing-induced CP one varies within $[0, 0.8]$. The strikingly different behavior of the CP asymmetries between the NP scenarios demonstrates that these observables can be used to distinguish between the scenarios.

3.3 Extracting Wilson coefficients from the CP asymmetries

We now go one step further and show how CP asymmetries in $B_d \to K_S\mu^+\mu^-$ can help us extract the complex values of the Wilson coefficients C_9 and C_{10}. As the coefficients are complex numbers, they have two degrees of freedom each and we need at least four observables to extract their values. For this analysis, we consider a minimal scenario with four observables, but we stress that additional observables would help overconstrain the system and produce a better fit. We consider:

- the CP-averaged branching ratio of $B^\pm \to K^\pm\mu^+\mu^-$ in the two q^2 bins of $q^2 \in [1.1, 6.0]$ and $q^2 \in [15, 22]$,
- the direct CP asymmetry of $B^\pm \to K^\pm\mu^+\mu^-$ in the q^2 bin of $[8, 9]$,
- the mixing-induced CP asymmetry of $B_d^0 \to K_S\mu^+\mu^-$ in the q^2 bin of $[1.1, 6.0]$.

These choices of bins play to the strengths of each observable. The direct CP asymmetry is chosen close to a $c\bar{c}$ resonance, where it can be maximally enhanced, while the branching ratios and mixing-induced CP asymmetry are chosen outside the resonance region, where they are robust with respect to uncertainties from hadronic long-distance effects.

For illustration, we consider Benchmark Point 2 of (10). Using this point to compute the values of our observables, we get

$$\begin{aligned} \mathcal{A}_{\rm CP}^{\rm dir}[8,9] &= 0.16 \pm 0.02\,, & \mathcal{A}_{\rm CP}^{\rm mix}[1.1,6] &= 0.94 \pm 0.04\,, \\ \mathcal{B}[1.1,6.0] &= (1.15 \pm 0.02) \times 10^{-7}\,, & \mathcal{B}[15,22] &= (0.908 \pm 0.018) \times 10^{-7}\,, \end{aligned} \tag{11}$$

where the uncertainties indicate a hypothetical future experimental scenario. We have here chosen the uncertainty on $\mathcal{A}_{\rm CP}^{\rm dir}$ to be about one third of the current experimental uncertainty in the nearest available q^2 bins [30]. For $\mathcal{A}_{\rm CP}^{\rm mix}$, we have chosen an uncertainy twice the size of that on the direct CP asymmetry. And for the uncertainties on the branching ratios, we have used 2%, again about one third of current experimental uncertainties [11]. Working with these uncertainties lets us explore how a given precision on observables translates into precision on the extracted Wilson coefficients. We do this by performing a chi-squared fit while setting theory uncertainties to zero. Fig. 4a shows the resulting 68% and 90% confidence level regions for the Wilson coefficients in the complex plane. We find that the corresponding observables let us determine the imaginary part of C_9 with high precision, but we get a less precise determination of C_{10}. The precision can be increased by over-constraining the system, for example by including additional q^2 bins, by considering new observables, or by assuming relations between the Wilson coefficients.

To show the precision gained from an over-constrained fit, we consider two scenarios with NP either in C_9 only or in $C_9 = -C_{10}$. For the C_9-only scenario, we use Benchmark Point 1 from (10) and obtain

$$\begin{aligned} \mathcal{A}_{\rm CP}^{\rm dir}[8,9] &= 0.15 \pm 0.02\,, & \mathcal{A}_{\rm CP}^{\rm mix}[1.1,6] &= 0.66 \pm 0.04\,, \\ \mathcal{B}[1.1,6.0] &= (1.16 \pm 0.02) \times 10^{-7}\,, & \mathcal{B}[15,22] &= (0.806 \pm 0.016) \times 10^{-7}\,, \end{aligned} \tag{12}$$

where the uncertainties again correspond to a hypothetical future scenario. With these inputs for C_9 only and those of (11) for $C_9 = -C_{10}$, we find the more precise confidence limits of Fig. 4b.

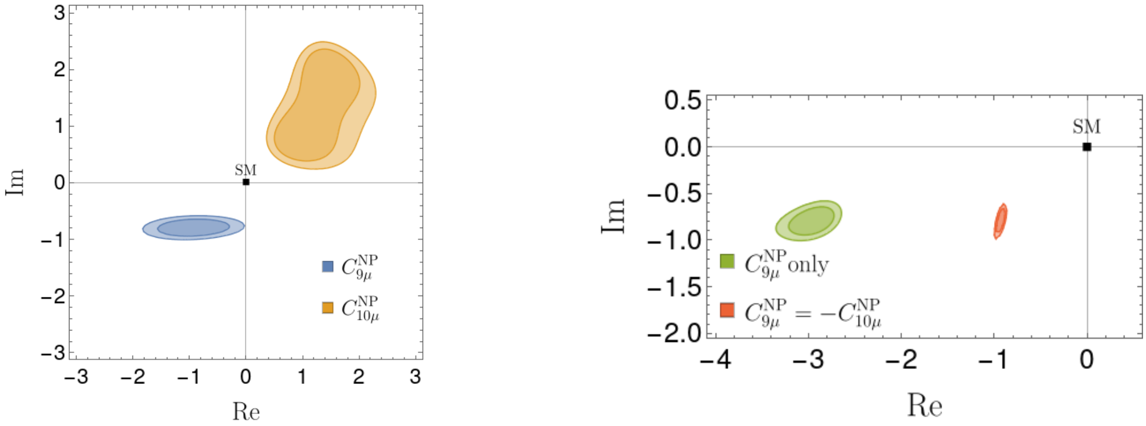

(a) Result from a fit treating the absolute values and phases of C_9^{NP} and C_{10}^{NP} as free parameters.

(b) Result from an overconstrained fit. The green region comes from assuming NP in C_9 only, while the red region comes from assuming $C_9 = -C_{10}$.

Figure 4: Extracted values of C_9 and C_{10} in the complex plane. The lines indicate the 68% and 90% confidence limits. (From [12].)

4. Testing electron–muon universality with CP violation

With current experimental data on R_K being in agreement with the SM prediction, is there still space left for electron–muon universality violation? If the Wilson coefficients in $B \to K\mu^+\mu^-$ and $B \to Ke^+e^-$ are the same, then we have electron–muon universality. However, as we will show in this section following [31], when we allow the coefficients to be complex, they can take different values while still respecting $R_K \sim 1$. We will first consider real coefficients and then complex ones, allowing for new sources of CP violation.

4.1 Real Wilson coefficients

To accommodate data on the branching ratio $\mathcal{B}(B^+ \to K^+\mu^+\mu^-)$ [11], a real $C_{9\mu}^{NP}$ has to take a value within

$$C_{9\mu}^{NP} = [-1.32, -0.40]C_9^{SM} \,. \tag{13}$$

We fix $C_{9\mu}^{NP}$ to a value within this range and then use the recent R_K measurement to compute what values are allowed for C_{9e}^{NP}. Fig. 5 shows the resulting plot, where the dashed vertical line shows the value that $C_{9\mu}$ is fixed to, the curve shows values of R_K as a function of C_{9e}^{NP}, and the horizontal band the experimental 1σ band for R_K. We observe that C_{9e} is forced to take one of two discrete values, one which is identical to $C_{9\mu}^{NP}$ and one which is not. As a result, if we assume real Wilson coefficients, the recent R_K data impose electron–muon universality up to a twofold ambiguity.

4.2 Complex Wilson coefficients

We now consider $C_{9\mu}^{NP}$ and C_{9e}^{NP} to be complex parameters, allowing for new sources of CP violation. Fig. 6 schematically illustrates our procedure: we first constrain $C_{9\mu}^{NP}$ using the branching ratio and direct CP asymmetry of $B^\pm \to K^\pm\mu^+\mu^-$, then use current R_K data to determine the allowed complex values of C_{9e}^{NP}, and finally show how these values translate into CP-violating observables.

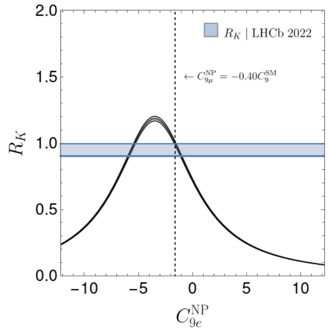

Figure 5: R_K as a function of a real $C_{9e}^{\rm NP}$, corresponding to no new sources of CP violation. (From [31].)

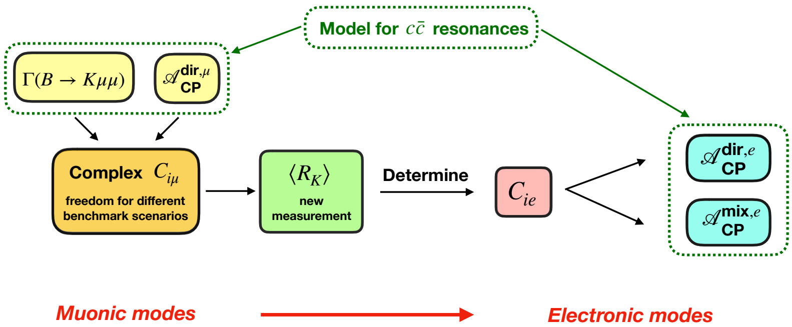

Figure 6: Illustration of our procedure to show how much space is left for electron–muon non-universality in $B \to K\ell^+\ell^-$ when we allow for new sources of CP violation. (From [31].)

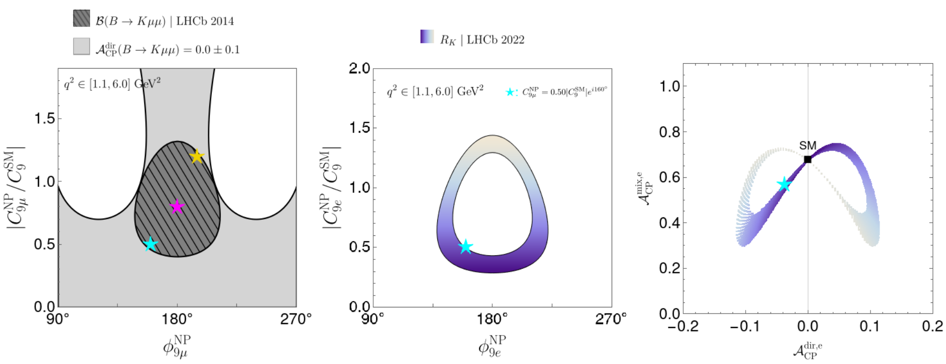

(a) **(b)** **(c)**

Figure 7: Constraints on a complex $C_{9\mu}^{\rm NP}$ (left), $C_{9e}^{\rm NP}$ (middle), and CP asymmetries in $B_d \to K_S e^+e^-$ (right). (From [31].)

Fig. 7a shows the experimental bounds on $C_{9\mu}^{\rm NP}$: The dark striped egg shows the bound from $\mathcal{B}(B^\pm \to K^\pm\mu^+\mu^-)$, and the light gray region shows the bound from $\mathcal{A}_{\rm CP}^{\rm dir}(B^\pm \to K^\pm\mu^+\mu^-)$. The direct CP asymmetry has been constrained by the LHCb collaboration in different bins of q^2 [25], and averaging over the bins yields the rather strict bound of $\mathcal{A}_{\rm CP}^{\rm dir}(B \to K\mu^+\mu^-) = 0.012 \pm 0.017$. However, by taking this average we implicitly assume that the CP asymmetry is constant over the q^2 spectrum. As shown in [26], this is not necessarily the case; any existing asymmetry will be enhanced by $c\bar{c}$ resonances and change across the spectrum. Because of this, we instead use the more conservative range of

$$\mathcal{A}_{\rm CP}^{\rm dir}(B^- \to K^-\mu^+\mu^-) = 0.0 \pm 0.1\,, \tag{14}$$

where we take the uncertainty to cover all the individual bins between 1.1 and 6.0 GeV^2 in [25].

For illustration, we fix $C_{9\mu}$ to the blue star, given by

$$C_{9\mu}^{\rm NP} = 0.50|C_9^{\rm SM}|e^{i160^\circ}\,, \tag{15}$$

and vary the electronic coefficient $C_{9e}^{\rm NP}$ to explore which values are consistent with R_K. Fig. 7b shows the result. We have coloured each point in the plot according to the absolute value of $C_{9e}^{\rm NP}$. If electron–muon universality were to hold in $B \to K\ell^+\ell^-$, then $C_{9e}^{\rm NP}$ should take the same value as $C_{9\mu}^{\rm NP}$—that is, the blue star. But that is not what the figure shows. Instead, the electronic coefficient can take any value within the blue, egg-shaped region. Even with a value of R_K close to one, there is still a lot of space left for electron–muon non-universality.

To probe this new parameter space, we need measurements of direct and mixing-induced CP asymmetries in $B_d \to K_S\mu^+\mu^-$ and $B_d \to K_S e^+e^-$. Fig. 7c shows how the allowed space in the $C_{9e}^{\rm NP}$ complex plane translates into the electronic CP asymmetry plane. The colour coding matches that of Fig. 7b and allows for easy comparison between the two planes. With data on either asymmetry, we can draw a band in the CP asymmetry plane, and with data on both we can draw two intersecting bands. If that intersection were to exclude a known value of $C_{9\mu}^{\rm NP}$ (in this case the blue star), that would constitute a clear signal of electron–muon universality violation.

The only data available so far on CP asymmetries in $B \to Ke^+e^-$ come from the Belle Collaboration, who measured the direct CP asymmetry of $B^\pm \to K^\pm e^+e^-$ and found [32]:

$$\mathcal{A}_{\rm CP}^{\rm dir,e} = 0.14 \pm 0.14\,, \tag{16}$$

which is an average over different q^2 bins. Given measurements also of the corresponding mixing-induced asymmetry of $B_d \to K_S e^+e^-$, we can use the method presented in [12] to determine the complex value of $C_{9e}^{\rm NP}$. Then, we would know whether or not electron–muon universality holds in these decays. Considering the significant room left for CP-violating couplings that violate electron–muon universality, we encourage the experimental community to perform detailed feasibility studies of the corresponding measurements.

We stress that these results are robust with respect to the specific benchmark value chosen for $C_{9\mu}^{\rm NP}$ and the particular NP scenario considered. To show this, in Fig. 8 we show the same plots as in Fig. 7 but for the NP scenario of $C_{9\ell}^{\rm NP} = -C_{10\ell}^{\rm NP}$ and red diamond benchmark point given by

$$C_{9\mu}^{\rm NP} = -C_{10\mu}^{\rm NP} = 0.40|C_9^{\rm SM}|e^{i130^\circ}\,. \tag{17}$$

We observe that also in this scenario, a large parameter space opens up for electron–muon non-universality that is consistent with the latest data on R_K.

PoS(CORFU2023)128

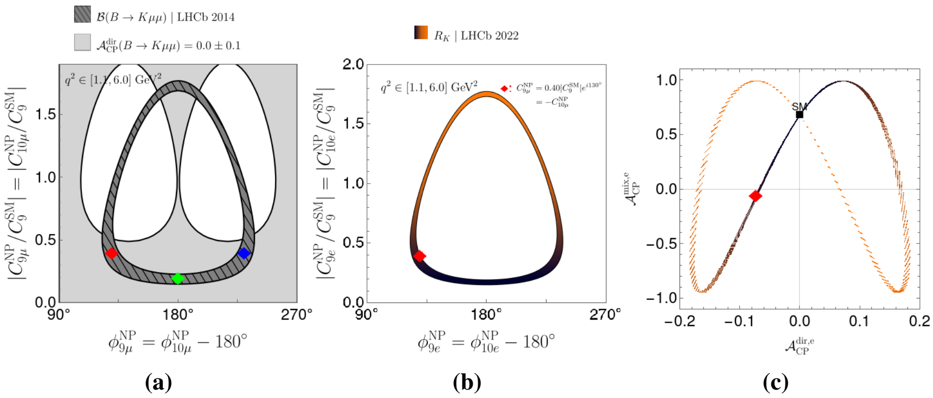

Figure 8: Same as Fig. 7 but for the NP scenario $C^{\rm NP}_{9\ell} = -C^{\rm NP}_{10\ell}$. (From [31].)

5. Conclusions

In studies of rare B-meson decays, new sources of CP violation are often neglected. We have included the effects of such new sources and presented two phenomena that arise in the process. First, we have shown how measurements of direct and mixing-induced CP violation in $B \to K\ell^+\ell^-$ decays can be used to extract the complex values of the Wilson coefficients $C_{9\ell}$ and $C_{10\ell}$. Second, we have demonstrated how new sources of CP violation open up a new parameter space for lepton flavour universality violation, allowing for significant violations of universality even with a value of R_K in agreement with the SM prediction. These studies provide exciting new opportunities to reveal New Physics effects in the coming high-precision era.

Acknowledgments

A.R. would like to thank the organizers for the invitation to the enjoyable conference. This research has been supported by the Netherlands Organisation for Scientific Research (NWO).

References

[1] C. Bobeth, M. Chrzaszcz, D. van Dyk and J. Virto, *Long-distance effects in $B \to K^*\ell\ell$ from analyticity*, *Eur. Phys. J. C* **78** (2018) 451, [1707.07305].

[2] A. K. Alok, B. Bhattacharya, A. Datta, D. Kumar, J. Kumar and D. London, *New Physics in $b \to s\mu^+\mu^-$ after the Measurement of R_{K^*}*, *Phys. Rev. D* **96** (2017) 095009, [1704.07397].

[3] A. Datta, J. Kumar and D. London, *The B anomalies and new physics in $b \to se^+e^-$*, *Phys. Lett. B* **797** (2019) 134858, [1903.10086].

[4] W. Altmannshofer and P. Stangl, *New physics in rare B decays after Moriond 2021*, *Eur. Phys. J. C* **81** (2021) 952, [2103.13370].

[5] M. Algueró, J. Matias, B. Capdevila and A. Crivellin, *Disentangling lepton flavor universal and lepton flavor universality violating effects in $b \to s\ell^+\ell^-$ transitions*, *Phys. Rev. D* **105** (2022) 113007, [2205.15212].

[6] N. Gubernari, M. Reboud, D. van Dyk and J. Virto, *Improved theory predictions and global analysis of exclusive $b \to s\mu^+\mu^-$ processes*, *JHEP* **09** (2022) 133, [2206.03797].

[7] L.-S. Geng, B. Grinstein, S. Jäger, S.-Y. Li, J. Martin Camalich and R.-X. Shi, *Implications of new evidence for lepton-universality violation in $b \to s\ell^+\ell^-$ decays*, *Phys. Rev. D* **104** (2021) 035029, [2103.12738].

[8] A. Carvunis, F. Dettori, S. Gangal, D. Guadagnoli and C. Normand, *On the effective lifetime of $B_s \to \mu\mu\gamma$*, *JHEP* **12** (2021) 078, [2102.13390].

[9] F. Mahmoudi, *Theoretical Review of Rare B Decays*, in *20th Conference on Flavor Physics and CP Violation* , 8, 2022. 2208.05755.

[10] N. R. Singh Chundawat, *CP violation in $b \to s\ell\ell$: a model independent analysis*, 2207.10613.

[11] LHCb collaboration, R. Aaij et al., *Differential branching fractions and isospin asymmetries of $B \to K^{(*)}\mu^+\mu^-$ decays*, *JHEP* **06** (2014) 133, [1403.8044].

[12] R. Fleischer, E. Malami, A. Rehult and K. K. Vos, *Fingerprinting CP-violating New Physics with $B \to K\mu^+\mu^-$*, *JHEP* **03** (2023) 113, [2212.09575].

[13] LHCb collaboration, R. Aaij et al., *Test of lepton universality using $B^+ \to K^+\ell^+\ell^-$ decays*, *Phys. Rev. Lett.* **113** (2014) 151601, [1406.6482].

[14] LHCb collaboration, R. Aaij et al., *Search for lepton-universality violation in $B^+ \to K^+\ell^+\ell^-$ decays*, *Phys. Rev. Lett.* **122** (2019) 191801, [1903.09252].

[15] LHCb collaboration, R. Aaij et al., *Test of lepton universality in beauty-quark decays*, *Nature Phys.* **18** (2022) 277–282, [2103.11769].

[16] M. Bordone, G. Isidori and A. Pattori, *On the Standard Model predictions for R_K and R_{K^*}*, *Eur. Phys. J. C* **76** (2016) 440, [1605.07633].

[17] LHCb collaboration, *Test of lepton universality in $b \to s\ell^+\ell^-$ decays*, 2212.09152.

[18] LHCb collaboration, *Measurement of lepton universality parameters in $B^+ \to K^+\ell^+\ell^-$ and $B^0 \to K^{*0}\ell^+\ell^-$ decays*, 2212.09153.

[19] G. Isidori, D. Lancierini, S. Nabeebaccus and R. Zwicky, *QED in $\overline{B} \to \overline{K}\ell^+\ell^-$ LFU ratios: theory versus experiment, a Monte Carlo study*, *JHEP* **10** (2022) 146, [2205.08635].

[20] S. Descotes-Genon, M. Novoa-Brunet and K. K. Vos, *The time-dependent angular analysis of $B_d \to K_S\ell\ell$, a new benchmark for new physics*, *JHEP* **02** (2021) 129, [2008.08000].

[21] W. Altmannshofer, P. Ball, A. Bharucha, A. J. Buras, D. M. Straub and M. Wick, *Symmetries and Asymmetries of $B \to K^*\mu^+\mu^-$ Decays in the Standard Model and Beyond*, JHEP **01** (2009) 019, [0811.1214].

[22] J. Gratrex, M. Hopfer and R. Zwicky, *Generalised helicity formalism, higher moments and the $B \to K_{J_K}(\to K\pi)\bar{\ell}_1\ell_2$ angular distributions*, Phys. Rev. D **93** (2016) 054008, [1506.03970].

[23] G. Buchalla, A. J. Buras and M. E. Lautenbacher, *Weak decays beyond leading logarithms*, Rev. Mod. Phys. **68** (1996) 1125–1144, [hep-ph/9512380].

[24] R. Fleischer, D. G. Espinosa, R. Jaarsma and G. Tetlalmatzi-Xolocotzi, *CP Violation in Leptonic Rare B_s^0 Decays as a Probe of New Physics*, Eur. Phys. J. C **78** (2018) 1, [1709.04735].

[25] LHCb collaboration, R. Aaij et al., *Measurement of CP asymmetries in the decays $B^0 \to K^{*0}\mu^+\mu^-$ and $B^+ \to K^+\mu^+\mu^-$*, JHEP **09** (2014) 177, [1408.0978].

[26] D. Bečirević, S. Fajfer, N. Košnik and A. Smolkovič, *Enhanced CP asymmetries in $B \to K\mu^+\mu^-$*, Eur. Phys. J. C **80** (2020) 940, [2008.09064].

[27] A. Smolkovic, *LFU and CP violation in $b \to s\mu\mu$*, PoS **ICHEP2022** (11, 2022) 715.

[28] K. De Bruyn, R. Fleischer, E. Malami and P. van Vliet, *New Physics in $B_q^0 - \bar{B}_q^0$ Mixing: Present Challenges, Prospects, and Implications for $B_q^0 \to \mu^+\mu^-$*, J. Phys. G: Nucl. Part. Phys. (8, 2022) , [2208.14910].

[29] LHCb collaboration, R. Aaij et al., *Measurement of the phase difference between short- and long-distance amplitudes in the $B^+ \to K^+\mu^+\mu^-$ decay*, Eur. Phys. J. C **77** (2017) 161, [1612.06764].

[30] R. Aaij, B. Adeva, M. Adinolfi, A. Affolder, Z. Ajaltouni, S. Akar et al., *Measurement of cp asymmetries in the decays $b^0 \to k^{*0}\mu^+\mu^-$ and $b^+ \to k^+\mu^+\mu^-$*, Journal of High Energy Physics **2014** (Sep, 2014) .

[31] R. Fleischer, E. Malami, A. Rehult and K. K. Vos, *New perspectives for testing electron-muon universality*, JHEP **06** (2023) 033, [2303.08764].

[32] Belle collaboration, J. T. Wei et al., *Measurement of the Differential Branching Fraction and Forward-Backward Asymmetry for $B \to K^{(*)}\ell^+\ell^-$*, Phys. Rev. Lett. **103** (2009) 171801, [0904.0770].